*Malaysian Journal of Chemistry, 2020, Vol. 22(4), 43-51*

# Facile Preparation of Two-Dimensional Sheet-Like Tin Disulfide

**Juan Matmin*, Fazira Ilyana Abdul Razak, Susilawati Toemen and Mohamad Shazwan Shah Jamil**
Department of Chemistry, Faculty of Science, Universiti Teknologi Malaysia (UTM), 81310 UTM Johor Bahru, Johor, Malaysia
*Corresponding author (e-mail: juanmatmin@utm.my)

Nanomaterials with two-dimensional (2D) arrangements displaying excellent electronic properties, sizable band gaps, and stable charge transfer applications are unique and highly desired. The 2D structures featuring sheet-like arrangements are typically prepared by harsh calcination of the salt precursors through a rapid temperature increase of more than 300ºC for a few hours, which restricts the upscale possibility. In light of this, we report on a facile preparation of tin disulfide ($SnS_2$) via direct heating methods using sunlight (SL), a light bulb (LB), and a hot plate (HP). These heating sources were selected to represent a natural irradiator, a least expensive illuminator, and the most common heater easily found in modern experimental setups which operates on low heating power to circumvent the sintering effects of conventional methods. The prepared $SnS_2$ series gave strong (001) facets on diffractogram designate for preferable crystal growth along a single stacking orientation. This strong stacking gave aggregations for both SL and LB-$SnS_2$ of the size less than 5 µm. In the case of HP-$SnS_2$, an interconnected sheet-like morphology composed of inter-layer $SnS_2$ structures having the nanosize of 870 nm was determined. These suggest that a certain amount of energy is required for an anisotropy crystallization of $SnS_2$ to promote the 2D sheet-like arrangements. The described facile preparation offers a great potential for a mild and large scale synthesis of 2D materials for advanced applications.

**Key words**: Tin disulfide; sheet-like arrangements; two-dimensional materials; facile preparation.

*Received: February 2020; Accepted: June 2020*

In recent years, two-dimensional (2D) nanomaterials from inorganic metals or graphene with sheet-like structures have displayed excellent electronic properties, sizable band gaps, and stable charge transfer applications for visible light photocatalysis. In this context, tin disulfide ($SnS_2$) is recognized as one of the most promising sheet-like materials, mainly because of its exclusive band gaps (1.9-2.5 eV). Moreover, $SnS_2$ is a famous n-type semiconductor for electrical conduction under visible light wavelengths (390 to 700 nm). Notably, these particular $SnS_2$ layers have already been found to be significant as photodetectors, semiconductors, and supercapacitor materials [1].

As a general rule, $SnS_2$ is prepared by calcination of the precursor mixtures of metal oxides or thiosulfates, thiourea, thioacetamide, and sulfur powders at above 300ºC, which are known as very high temperatures, resulting in undesired irregular shapes and facets [2,3]. Typical preparations for $SnS_2$ involve thermal evaporation, electrodeposition, spray pyrolysis technique, chemical bath deposition, sputtering, and many more, which are strongly dependent on the presence of thermo-derived methods [4,5]. To assist better understanding, the various reports and their findings on the preparation of $SnS_2$ using various techniques are summarized in Table 1.

Unfortunately, most of the available thermo-derived methods suffer from sintering effects and result in particles agglomerations at micron sizes due to the excessive heating. Alternatively, recent works developed facile preparations of 2D materials using direct heating methods with low heating power such as sunlight, light bulbs or hot plates. These heating sources are selected to represent a natural irradiator, a least expensive illuminator, and the most common heater widely used in modern experimental setups. Nevertheless, there is no scientific works to investigate what types of materials could be prepared by using the direct heating methods, especially on 2D nanomaterials. As far as we are concerned, it is in high demand to prepare the sheet-like of 2D $SnS_2$ under mild conditions from the direct solid-state reaction of the corresponding precursors. For the first time, we compared different direct heating methods of sunlight, a light bulb, and a hot plate for the preparation of 2D nanomaterials. The goal of this study was to synthesize 2D $SnS_2$ by sunlight, a light bulb, and a hot plate as the direct heating methods and investigate their corresponding physicochemical properties. This work is crucial to establish a facile preparation method under low heating power.

**Table 1.** Preparation methods and corresponding morphologies on synthesis of $SnS_2$

| Compounds | Preparation methods | Morphologies | Reference |
|---|---|---|---|
| $SnS_2$ thin film | Coevaporation under Ar flow on $SiO_2$ substrates held at 600°C | Large flakes ranges from 40 to 70 µm | Yang *et al.* (2015) [6] |
| Layered $SnS_2$ | Calcination at 300°C for 5 h under argon atmosphere | Bulk layered structure with more than 1 µm | Chia *et al.* (2016) [5] |
| $SnS_2$ nanosheets | Calcination using Teflon-lined stainless steel autoclave at 220°C for 12 h | Sheet-like structure with quasi-hexagonal stacking of less than 2 µm | Yu *et al.* (2014) [7] |
| $SnS_2$ nanoflakes | Calcination at 240°C for 10 h | Lamellar flake-like morphology of more than 1 µm | Zhang *et al.* (2010) [8] |
| $SnS_2$ nanosheets arrays sandwiched | Sealed Teflon-lined stainless steel autoclave and atomic layer deposition (ALD) reactor | Sandwiched structure with thickness about 75 - 95 nm | Ren *et al.* (2017) [9] |

Herein, we successfully developed a facile preparation of 2D sheet-like $SnS_2$ based on several direct-heating methods. In this work, tin(IV) chloride pentahydrate, $SnC_{l4}.5H_2O$, and thioacetamide (TAA) precursors were treated under a series of heating sources such as sunlight (SL), bulb (LB), and hot plate (HP) heating at less than 150ºC to avoid the harsh calcination procedure. Interestingly, $SnS_2$ has been demonstrated as a catalyst for photodegradation of methylene blue under UV irradiation.

## EXPERIMENTAL

Tin(IV) chloride pentahydrate (98%, Sigma Aldrich, St. Louis, MO, USA), thioacetamide (TAA, 99%, Acros, NJ, USA), isopropyl alcohol (Tedia, Fairfield, CT, USA), ethanol (99%, Fisher Chemicals, NH, USA), and hydrochloric acid (HCl, 36.5-38.0%, JT Baker, A.C.S. Reagen, USA) were purchased and used without additional pre-treatments.

Firstly, 0.45 g of $SnCl_4.5H_2O$ and 0.33 g of TAA were dissolved in 30 mL of isopropyl alcohol in a closed-capped test tube. The solution was then transferred into a sample tube after 30 min of vigorous stirring. Later, the collected precipitates were centrifuged in a mixture of water and ethanol to yield yellowish-gold solids. Then, the solids were acidified by adding 2 mL of 0.1 M HCl. For the direct heating methods, the precursors' samples were introduced to different heat sources such as sunlight (SL), light bulb (LB), and hot plate (HP). To prepare SL-$SnS_2$, 5.0 g of samples were exposed to direct sunlight under continuous stirring for 6 h before drying off. For LB-$SnS_2$, 5.0 g of samples were illuminated under a light bulb (25 W) with continuous stirring for 6 h. In the preparation of HP-$SnS_2$, 5.0 g of samples were heated at 120°C on a hot plate in glycerin as a medium with continuous stirring for 6 h.

To characterize the $SnS_2$ samples, an X-ray diffractometer (XRD, Ultima IV, Rigaku Corporation, Japan) with Cu Kα radiation ($\lambda$ = 1.54 Å) at 30 kV voltage and 15 mA current was utilized. The particle size measurements were carried out using HELOS Rados laser diffraction to give the average size distribution (Sympatec Gmbh, Clausthal-Zellerfeld, Germany). The morphology of the samples was analyzed using a field emission scanning electron microscopy (FESEM, JSM-6700F, JEOL, Tokyo, Japan). Transmission electron microscopy (TEM) micrographs of the samples were obtained with JEM-2100F Electron Microscope (JEOL, Tokyo, Japan). Fourier-transform infrared (FTIR) spectrometer analysis was carried out on disc-pallet samples, scanned at a resolution of 4 $cm^{-1}$ over a wavenumber range of 450 to 4000 $cm^{-1}$ using a FTIR spectrometer (Spectrum RX1 FTIR system, Perkin Elmer, Waltham, M.A., USA). Fluorescence spectra were determined by photoluminescent (PL) spectroscopy (JASCO FP-8500, Tokyo, Japan).

For the photocatalytic testing, a suspension consisting of 2.0 mL of 0.1 mM methylene blue was added to 50 mg of each $SnS_2$ in a quartz cuvette. The mixture was stirred in the dark for 180 min to ensure an adsorption-desorption balance. The absorption spectra were recorded at 60 min intervals at room temperature via time-dependent UV–Vis. The photodegradation of methylene blue was monitored from decreasing UV−Vis intensity at an absorption band of 638 nm.

## RESULTS AND DISCUSSION

The crystalline state and phase composition of all $SnS_2$ were characterized by XRD as shown in Figure 1. Based on Figure 1, all the XRD peak positions were accurately indexed with the standard diffraction data of JCPDS no. 23-0677 [4]. This indicated a hexagonal type of $SnS_2$ (space group $P\bar{3}m1$) with cell parameters of a = b = 3.659 Å and c = 5.879 Å. The presence of strong reflections and the absence of impurity peaks indicated good purity of crystalline materials [10,11]. All of the $SnS_2$ samples displayed a prominent diffraction peak at 2θ = 15.0°, which can be assigned to the hexagonal crystal at (001) facet. By using the Bragg's Law, as in equation (1), the d-spacing (2θ = 15.0°) of the sheet-like $SnS_2$ was estimated at 5.9 Å from the XRD measurements:

$$2d \sin\theta = n\lambda \qquad (1)$$

Where n is a positive integer and λ is the wavelength of the incident wave. Furthermore, several distinguished peaks at 2θ = 15.0°, 28.2°, 32.1°, and 41.9° assigned for (002), (003), and (004) planes were also determined. By using the Scherrer equation, as in equation (2), from the measurement at (2θ = 15.0°) for (001) peak, the crystal size of the sheet structures was measured at ~70 nm.

$$d = \frac{k\lambda}{\beta \cos\theta} \qquad (2)$$

Where θ is the Bragg diffraction angle, β is the full width at the half-height maxima (FWHM) of the desired XRD peaks, k is the Scherrer constant of 0.9 for typical crystallites, λ is the X-ray wavelength of Cu Kα, and d is the particle size of the crystal. From the XRD diffractions, HP-$SnS_2$ demonstrated the strongest reflection at (001) planes as compared to other samples, which might be due to good anisotropic arrangements from preferred sheet-like stacking. According to the Bravais Lattice, as in equation (3), the lattice constants of cell parameters were measured at a= b= 3.589 ± 0.001 Å and c= 5.862 ± 0.004 Å, with c/a ratio and atomic packing factor of 1.633 and 0.74, respectively,

$$\frac{1}{d_{hkl}^2} = \frac{4}{3}\left(\frac{h^2 + hk + k^2}{a^2}\right) + \frac{l^2}{c^2} \qquad (3)$$

Where d is the distance of adjacent planes (h k l) and a and c are the lattice parameters of the hexagonal structure. Based on the XRD measurements, it can, therefore, be deduced that the aggregation growth and self-assembly of $SnS_2$ are preferentially induced along (001) plane led by solvents and precursors characteristics [1,12].

To further corroborate the structural analysis of $SnS_2$, the FTIR measurements were carried out and their corresponding spectra are shown in Figure 2. Based on Figure 2, all of the prepared $SnS_2$ samples exhibited almost similar FTIR spectra showing the vibrational band at 628 $cm^{-1}$ ascribed to the Sn-S bond. As can be seen, broad bands from 3400 to 1633 $cm^{-1}$ can be assigned to hydrogen-bonded hydroxyl groups (O–H) vibration indicating strong water bounds by intermolecular hydrogen bonding in the $SnS_2$ sheet-like structures, in full agreement with the literature [13,14].

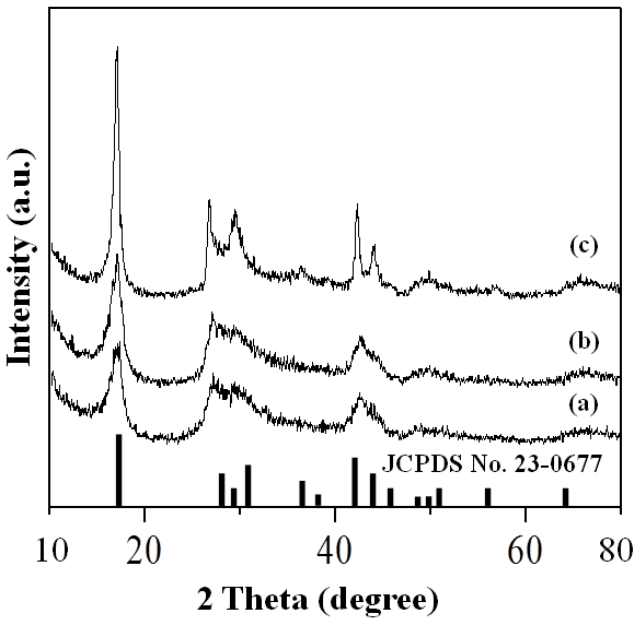


**Figure 1.** XRD patterns for (a) SL-$SnS_2$, (b) LB-$SnS_2$, and (c) HP-$SnS_2$

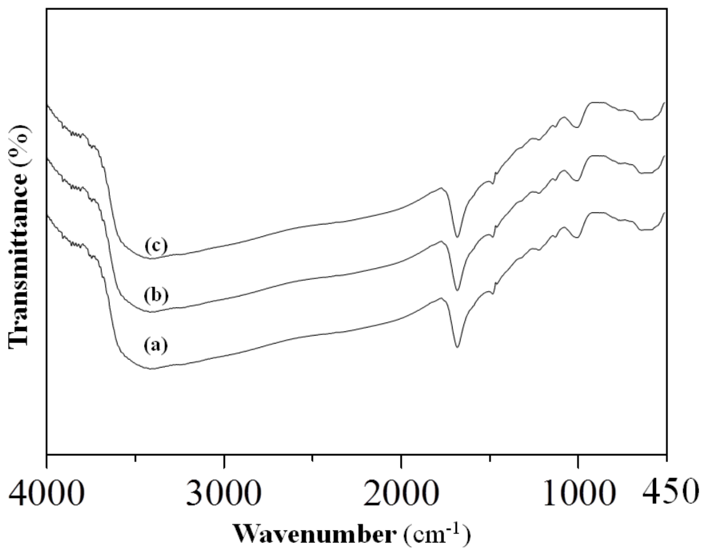


**Figure 2.** FTIR spectra for (a) SL-$SnS_2$ (b) LB-$SnS_2$, and (c) HP-$SnS_2$

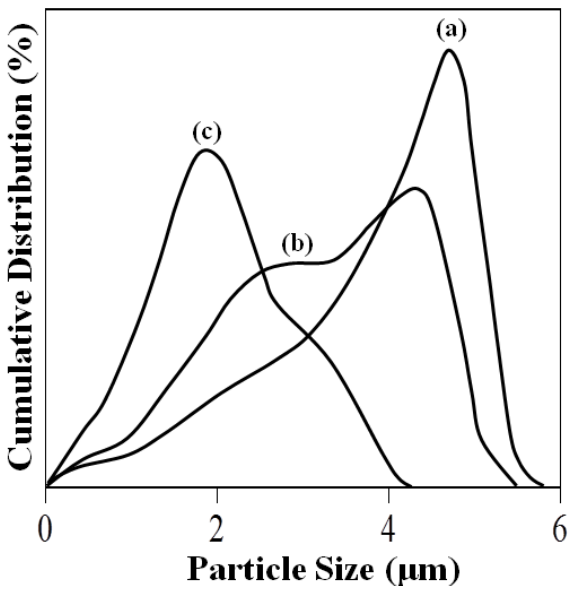


**Figure 3**. Average density distribution curves for (a) SL-$SnS_2$, (b) LB-$SnS_2$, and (c) HP-$SnS_2$

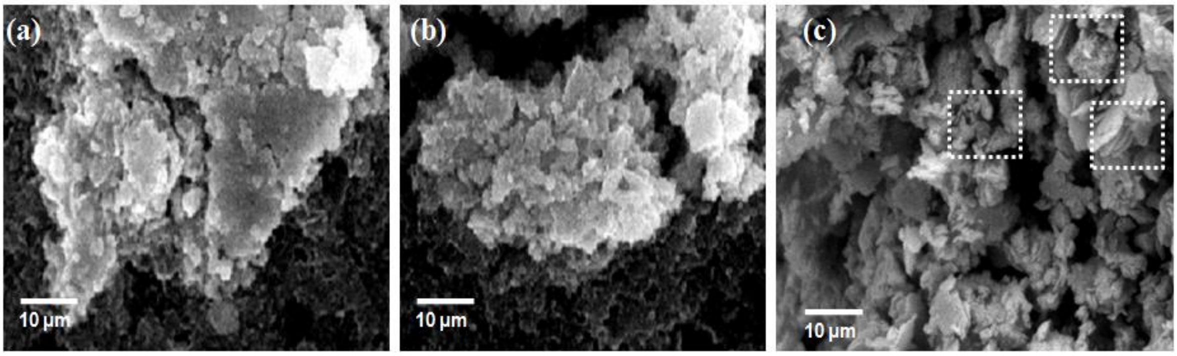


**Figure 4.** FESEM images for (a) SL-$SnS_2$, (b) LB-$SnS_2$, and (c) HP-$SnS_2$ with dotted box representing the selected inter-layered structured images

To quantify the average particle size, Figure 3 shows the particle size distribution for the prepared $SnS_2$. Based on Figure 3, the measured average particle size was found to be 4.08, 2.27, and 0.87 µm, corresponding to SL-$SnS_2$, LB-$SnS_2$ and HP-$SnS_2$, respectively. Moreover, the distribution curves showed a typical binomial-like distribution for all samples. The monomodal with a high amount samples dispersed at the centered of the mean region is significant for normal density distribution curve. Notably, the sheet-like $SnS_2$ consists of two layers of hexagonal closed-packed S anions with Sn cations adjacent to S–Sn–S sandwich ordering strongly held together by van der Waals interactions which directly affect the particle distributions [13].

FESEM analysis was used to monitor the textural morphology of $SnS_2$ as shown in Figure 4. The presence of large-scale entities and random distributions of non-uniform aggregates were observed in all samples. In particular, both FESEM images for SL-$SnS_2$ and BL-$SnS_2$ (Figures 4(a) and (b)) showed almost similar heavily aggregated materials of the size less than 5 µm. For HP-$SnS_2$, the FESEM image in Figure 4(c) shows inter-layered morphology composed of interconnected sheet-like $SnS_2$, as suggested by Mondal and co-workers [12]. Also, the size between each sheet of HP-$SnS_2$ was measured at 300 to 900 nm and the thickness of the sheet-like structures was determined at 70 to 90 nm. In addition, HP-$SnS_2$ displayed a pseudo-hexagonal sheet-like morphology having measurable and regular boundaries that were free from the presence of by-product particles on their surfaces [3]. This result is in a good agreement with the XRD analysis, implying their well-ordered monocrystalline characteristic.

To provide a better view on the morphology of $SnS_2$, TEM images were presented in Figure 5. Clearly, the TEM images for all samples show aggregates in layered morphology found in typical 2D nanomaterials. We can also see the large aggregates made up of multiple nanosheets in all $SnS_2$ samples. In particular, Figure 5(c) gives pseudo-hexagonal sheet with inter-layer morphology indicating a good formation of 2D layered crystals for HP-$SnS_2$, as supported from XRD and FESEM analyses. The presence of different morphologies for SL-$SnS_2$, LB-$SnS_2$, and HP-$SnS_2$ can be explained based on the formation mechanism. In the early stages, the $SnS_2$ particles nucleate and grow according to the Ostwald ripening processes. Nonetheless, the random distribution of non-uniform aggregates in both SL-$SnS_2$ and LB-$SnS_2$ might be due to the reactions in low energy for kinetically unfavorable anisotropic growth [15]. On the contrary, for HP-$SnS_2$, the nanosheets grew thicker and larger as the ripening development obeyed the intrinsic existence of hexagonal berndtite $SnS_2$ in stacked layers [11], which is in good agreements with the morphology and crystal structure analyses. The optical property for $SnS_2$ was investigated using PL, as shown in Figure 6. Furthermore, the optical band gap energy ($E_g$) can be determined using the photoelectric effect formula, as in equation (4).

$$E_g = \left(\frac{1240}{\lambda}\right)\ \text{eV} \qquad (4)$$

Where λ is the excitation wavelength in nm measured from PL. In Figure 6, the PL spectra show strong excitation peaks at 498.5 nm, indicating charge migration from recombination of excitons of the conduction band to the valence band. The signals are attributed to the excitonic PL, which is due to the nanosheet defects and surface oxygen vacancy. Also, the PL intensity in Figure 6 decreases as the average particle size increases, which is attributed to an increase in the nanosheet defects and decrease in surface oxygen vacancy. More importantly, the $E_g$ was estimated directly at 2.49 eV using equation (4) for all $SnS_2$, which indicated a semiconductor material that is highly active in the UV regions (λ = 280 nm).

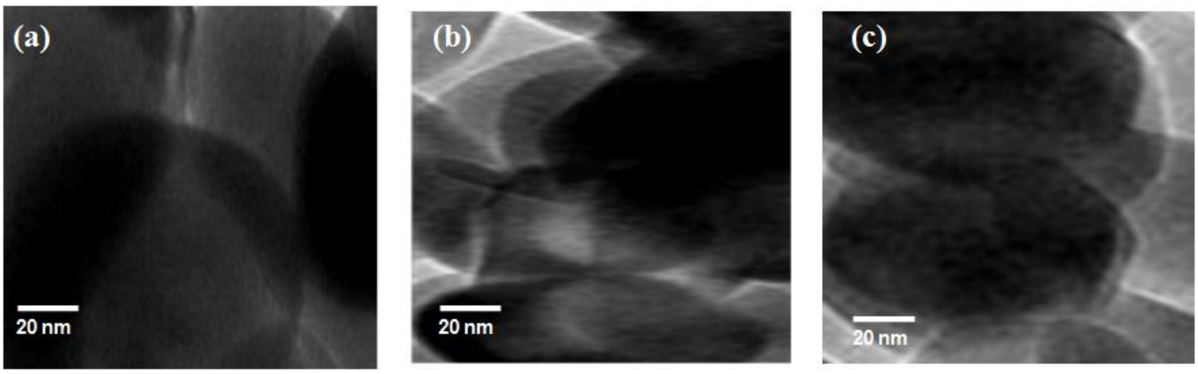


**Figure 5.** TEM images for (a) SL-$SnS_2$, (b) LB-$SnS_2$, and (c) HP-$SnS_2$

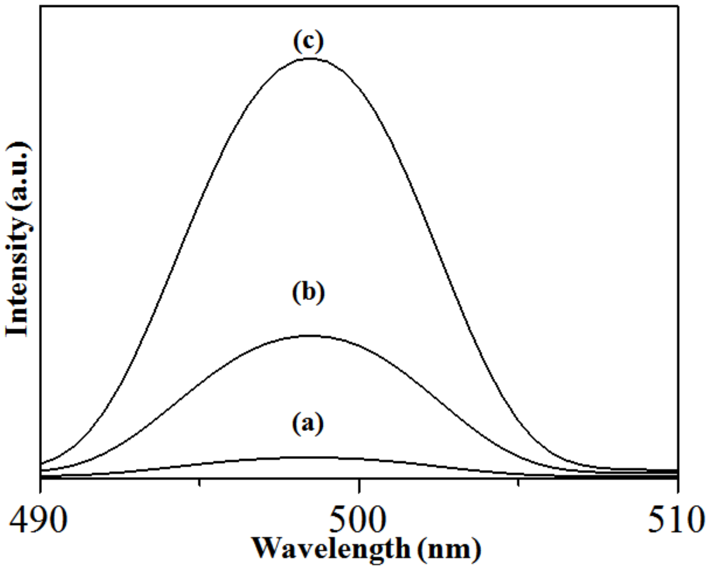


**Figure 6**. PL for (a) SL-$SnS_2$ (b) LB-$SnS_2$ and (c) HP-$SnS_2$ measured from λ excitation at 280 nm.

$SnS_2$ has narrower band gap energy, better thermal resistant, higher chemical stability, and non-toxic as compared to most layered structures such as CdS, SnS or graphene, which make it a preferred candidate for visible-light-responsive photocatalysis [16,17,18]. Previously, researchers had reported broader band gaps for CdS, SnS, and graphene of ~2.4 eV, ~2.3 eV, and 3.8 eV, respectively [19,20,21]. The narrow band gap energy of $SnS_2$ from 1.9 to 2.5 eV might be due to the unique 2D multi-sheet like structure. Moreover, recent works on $SnS_2$ had developed enhanced photocatalysts under visible light irradiation due to $SnS_2$ tremendous charge migration potential [2]. Taking this into consideration, as shown in Figure 7, we evaluated the catalytic performance of the prepared $SnS_2$ on the degradation of methylene blue by using equation (5) [22,23].

$$\text{Percentage of degradation } (\%) = \left(\frac{Co - Ct}{Co}\right) \times 100\% \qquad (5)$$

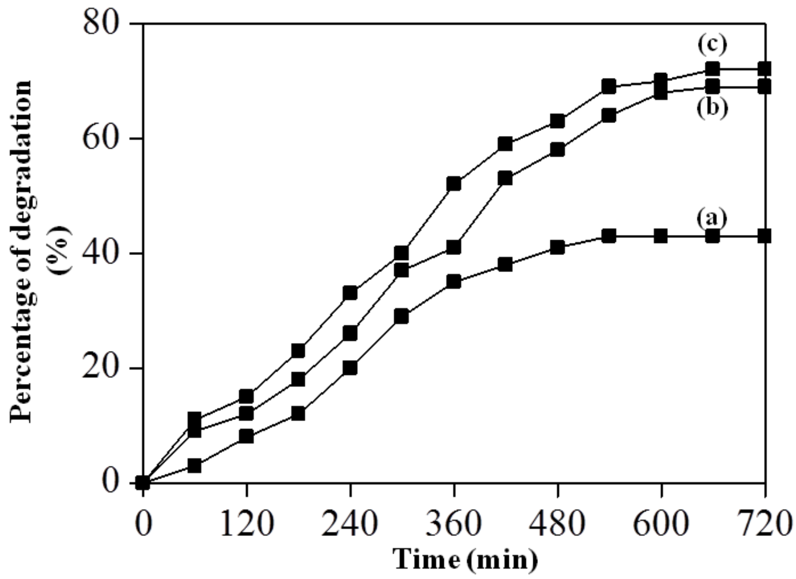


**Figure 7.** Degradation (%) against time plot of methylene blue in the presence of (a) SL-$SnS_2$ (b) LB-$SnS_2$, and (c) HP-$SnS_2$

Where C is the concentration at the start, o and measured time, t. Based on Figure 7, during the first 60 min, the dye directly degraded to 3%, 9%, and 11% on continuous mixing with SL-$SnS_2$, LB-$SnS_2$, and HP-$SnS_2$, respectively. Notably, HP-$SnS_2$ demonstrated the highest total degradation of 72%, followed by LB-$SnS_2$ and SL-$SnS_2$ of 69% and 43%, respectively. Based on the degradation results, the inter-layered morphology composed of interconnected sheet-like structures in HP-$SnS_2$ facilitated the photocatalytic activity. The improved photocatalytic performance in HP-$SnS_2$ was also due to its smallest average particle sizes (70 to 90 nm) that contributed to the highest surface oxygen vacancy and lowest nanosheet defects. After 720 min, a stable degradation plateau was observed suggesting that the series of $SnS_2$ prepared could be used as reliable photocatalysts. It is worth mentioning that further optimization is been carried out to realize the matter.

The proposed reaction mechanism of the $SnS_2$ photocatalyst under UV light irradiation for photodegradation of methylene blue is depicted in Figure 8. Briefly, the electron excitation from valence to conduction band produces holes in the valence band that react with methylene blue. In actual fact, $SnS_2$ holds a mixed character for electronic bands of metal d-orbitals and p-orbitals of the chalcogen group. In the presence of UV light, valence band (VB) electrons ($e^-$) in $SnS_2$ are excited to the conduction band (CB) at the same time as creating holes ($h^+$) in the VB. Later, the photoinduced holes in VB have a high oxidizing ability to oxidize the methylene blue. For HP-$SnS_2$, the sheet-like structures are ideal active sites for the efficient migration of $e^-$ and $h^+$ to surface reactions which justify the enhanced photodegradation activity. As reported by others, the final products for photodegradation of methylene blue are carbon dioxide, sulfate, nitrate, and water [11,24].

## CONCLUSION

A series of $SnS_2$ was successfully prepared under the mild condition from the direct-heating method of different sources using sunlight (SL), a light bulb (LB) and a hot plate (HP). Strong (001) facets from XRD diffractogram indicating preferential crystal growth orientation and similar IR spectra were measured for all of the $SnS_2$. Specifically, HP-$SnS_2$ displayed a very distinct morphology made up of interconnected sheet-like morphology as observed by FESEM and TEM analyses, compared to the randomly aggregated morphology for both SL and LB-$SnS_2$. The measured average particle size was found to be 4.08, 2.27, and 0.87 μm, corresponding to SL-$SnS_2$, LB-$SnS_2$ and HP-$SnS_2$, respectively. We also demonstrated the preliminary works on photocatalytic activity of the degradation of methylene blue as polluting dye. In the future, the facile preparation presented here is expected to offer a feasible procedure on the green protocol for the preparation of 2D sheet-like materials for possible batteries, water splitting technologies, and photodetectors development.

## ACKNOWLEDGEMENT

The authors highly acknowledge the financial support from Fundamental Research Grant Scheme (FRGS) from Higher Education Department, Ministry of Education (MOE), Malaysia through R.J130000.7826.4F957 and FRGS/1/2018/STG 07/UITM/03/5. Juan Matmin wishes to thank the support he received through UTM-ER under grant no. Q.J130000.2654.18J18.

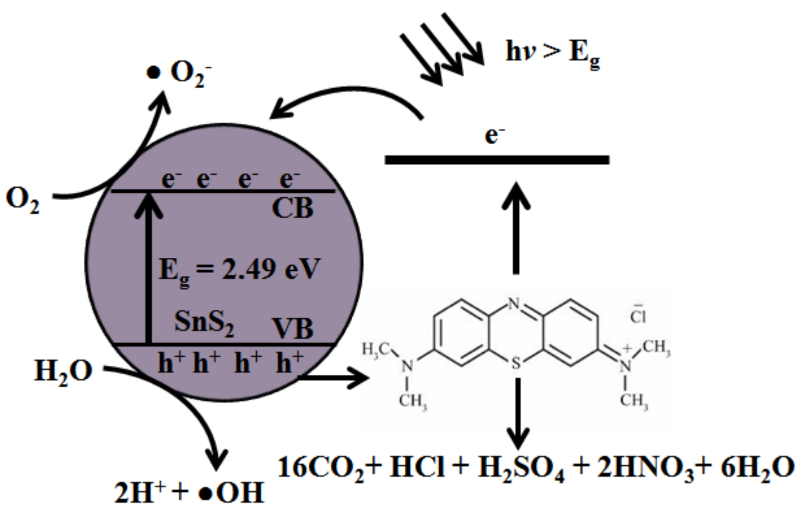


**Figure 8.** The proposed photodegradation mechanism of methylene blue using $SnS_2$ under UV light irradiation

REFERENCES


1. Parveen, N., Ansari, S. A., Alamri, H. R., Ansari, M. O., Khan, Z. and Cho, M. H. (2018) Facile synthesis of $SnS_2$ nanostructures with different morphologies for high-performance supercapacitor applications, ACS Omega, **3(2)**, 1581–1588.

2. Qin, N., Jing, K., Chen, R., Xiong, J., Liang, R., Li, Z. and Wu, L. (2017) $SnS_2$ nanoplates/$SnO_2$ nanotubes composites as efficient visible light-driven photocatalysts for Cr (VI) reduction. Research on Chemical Intermediates, **43(9)**, 5217–5228.

3. Fu, W., Wang, J., Zhou, S., Li, R. and Peng, T. (2018) Controllable fabrication of regular hexagon-shaped $SnS_2$ nanoplates and their enhanced visible-light-driven $H_2$ production activity. ACS Applied Nano Materials, **1(6)**, 2923–2933.

4. Dong, Y., Cai, G., Zhang, Q., Wang, H., Sun, Z., Wang, H., Wang, Y. and Xue, S., (2018) Solution-phase deposition of SnS thin films via thermo-reduction of $SnS_2$. Chemical Communications, **54(16)**, 1992–1995.

5. Chia, X., Lazar, P., Sofer, Z., Luxa, J. and Pumera, M. (2016) Layered SnS versus $SnS_2$: valence and structural implications on electrochemistry and clean energy electro-catalysis. The Journal of Physical Chemistry C, **120(42)**, 24098–24111.

6. Yang, Y. B., Dash, J. K., Littlejohn, A. J., Xiang, Y., Wang, Y., Shi, J., Zhang, L. H., Kisslinger, K., Lu, T. M. and Wang, G. C. (2016) Large single crystal $SnS_2$ flakes synthesized from coevaporation of Sn and S. Crystal Growth & Design, **16(2)**, 961–973.

7. Yu, J., Xu, C. Y., Ma, F. X., Hu, S. P., Zhang, Y. W. and Zhen, L. (2014) Monodisperse $SnS_2$ nanosheets for high-performance photocatalytic hydrogen generation. ACS Applied Materials & Interfaces, **6(24)**, 22370–22377.

8. Zhang, Y. C., Du, Z. N., Li, S. Y. and Zhang, M. (2010) Novel synthesis and high visible light photocatalytic activity of $SnS_2$ nanoflakes from $SnCl_2{\cdot}2H_2O$ and S powders. Applied Catalysis B: Environmental, **95(1-2)**, 153–159.

9. Ren, W., Zhang, H., Guan, C. and Cheng, C. (2018) $SnS_2$ nanosheets arrays sandwiched by N-doped carbon and $TiO_2$ for high-performance Na-ion storage. Green Energy & Environment, **3(1)**, 42–49.

10. Liu, H., Liu, Y., Wang, Z. and He, P. (2010) Facile synthesis of monodisperse, size-tunable SnS nanoparticles potentially for solar cell energy conversion. Nanotechnology, **21(10)**, 105707.

11. Matmin, J., Jalani, M. A., Osman, H., Omar, Q., Ab'Lah, N., Elong, K. and Kasim, M. F. (2019) Photochemical Synthesis of Nanosheet Tin Di/Sulfide with Sunlight Response on Water Pollutant Degradation. Nanomaterials, **9(2)**, 264.

12. Mondal, C., Ganguly, M., Pal, J., Roy, A., Jana, J. and Pal, T. (2014) Morphology controlled synthesis of $SnS_2$ nanomaterial for promoting photocatalytic reduction of aqueous Cr (VI) under visible light. Langmuir, **30(14)**, 4157–4164.

13. Park, S., Park, J., Selvaraj, R. and Kim, Y. (2015) Facile microwave-assisted synthesis of $SnS_2$ nanoparticles for visible-light responsive photocatalyst. Journal of Industrial and Engineering Chemistry, **31**, 269–275.

14. Taleblou, M., Borhani, E., Yarmand, B. and Kolahi, A. (2018) Structural and optoelectrical properties of single phase $SnS_2$ thin films at various substrate temperatures by Spray Pyrolysis. Iranian Journal of Materials Science and Engineering, **15(3)**, 43–52.

15. Min, Y., Moon, G. D., Kim, C. E., Lee, J. H., Yang, H., Soon, A. and Jeong, U. (2014) Solution-based synthesis of anisotropic metal chalcogenide nanocrystals and their applications. Journal of Materials Chemistry C, **2(31)**, 6222–6248.

16. Oliva, A. I., Solıs-Canto, O., Castro-Rodrıguez, R. and Quintana, P. (2001) Formation of the band gap energy on CdS thin films growth by two different techniques. Thin solid films, **391(1)**, 28–35.

17. Jain, P. and Arun, P. (2013) Influence of grain size on the band-gap of annealed SnS thin films. Thin Solid Films, **548**, 241–246.

18. Xu, X., Liu, C., Sun, Z., Cao, T., Zhang, Z., Wang, E., Liu, Z. and Liu, K. (2018) Interfacial engineering in graphene bandgap. Chemical Society Reviews, **47(9)**, 3059–3099.

19. Tao, H., Zhang, Y., Gao, Y., Sun, Z., Yan, C. and Texter, J. (2017) Scalable exfoliation and dispersion of two-dimensional materials–an update. Physical Chemistry Chemical Physics, **19(2)**, 921–960.

20. Sun, Y., Cheng, H., Gao, S., Sun, Z., Liu, Q., Liu, Q., Lei, F., Yao, T., He, J., Wei, S. and Xie, Y. (2012) Freestanding tin disulfide single-layers realizing efficient visible-light water splitting. Angewandte Chemie International Edition,

**51(35)**, 8727–8731.

21. Li, M., Liu, E., Hu, H., Ouyang, S., Xu, H. and Wang, D. (2014) Surfactant-free synthesis of single crystalline $SnS_2$ and effect of surface atomic structure on the photocatalytic property. International Journal of Photoenergy, 1–**7**.

22. Matmin, J., Affendi, I., Ibrahim, S. I. and Endud, S. (2018) Additive-free rice starch-assisted synthesis of spherical nanostructured hematite for degradation of dye contaminant. Nanomaterials, **8(9)**, 702.

23. Ahmad, M., Khan, M. Y., Sadaf, S., Iqbal, S., Nawaz, F. and Iqbal, J. (2019) Novel indigo-dye-doped graphene-supported $Mn/WO_3$ nanocomposite as visible light photocatalyst for degradation of methylene blue dye. Materials Research Express, **6(5)**, 1–12.

24. Calzada, L. A., Castellanos, R., García, L. A. and Klimova, T. E. (2019) $TiO_2$, $SnO_2$ and ZnO catalysts supported on mesoporous SBA-15 versus unsupported nanopowders in photocatalytic degradation of methylene blue. Microporous and Mesoporous Materials, **285**, 247–258.